Acoustically driven particle delivery assisted by a graded grating plate

Xiangxiang Xia,[1] Qian Yang,[1] Hengyi Li,[1] Manzhu Ke,[1,a)] Shasha Peng,[1] Chunyin Qiu,[1] and Zhengyou Liu[1,2]
[1]*Key Laboratory of Artificial Micro- and Nano-Structures of Ministry of Education and School of Physics and Technology, Wuhan University, Wuhan 430072, China*
[2]*Institute for Advanced Studies, Wuhan University, Wuhan 430072, China*

(Received 6 April 2017; accepted 20 June 2017; published online 18 July 2017)

Acoustic manipulation of particles, as a non-contact and non-damage method, has attracted much interest in recent years. Here, we present a platform for sound-driven particle delivery realized on an artificially engineered metal plate with manipulated, graded acoustic field distribution. By fabricating gratings with graded height on one surface of the structured plate, we obtain graded acoustic pressure distribution near the smooth surface of the plate. The acoustic field can be tuned at different positions by regulating the operating frequency, which originates from the gratings of different heights corresponding to different resonant frequencies. Therefore, from the effect of the acoustic radiation force exerted by this gradient field, a particle will transfer on the plate just by the frequency being tuned, without moving the acoustic source. Our theoretical analysis agrees well with the experimental demonstration. This work will lead to potential applications in drug delivery and microfluidics. *Published by AIP Publishing*. [http://dx.doi.org/10.1063/1.4991525]

Particle manipulation is very important for applications in fields such as physics, biology, and biomedical and medical sciences. Optical trapping and acoustic trapping on particles were realized by Ashkin in the early 1970s[1] and Wu in the early 1990s,[2] respectively. Since these developments, particle manipulation by optical forces[3–7] and acoustic forces[8–28] has attracted a great deal of research attention. Compared with optical tweezers, acoustic tweezers have several advantages: lower power consumption, weaker biological damage, and deeper penetration depth in light opaque media. Therefore, the acoustic manipulation of particles uses the acoustic radiation force (ARF) to provide a contactless and harmless handling method for particles suspended in a fluid. In the last two decades, the acoustic handling of a wide variety of particles such as solid microbeads,[8,14–16,27] droplets,[17,25] bubbles,[10,11,16] and biological cells[8,9,11–13,15,16] has been demonstrated, and different manipulation strategies and techniques have been accomplished such as particle separation,[9,22] trapping,[18–23] moving,[24–27] and concentration.[14] However, most of the abovementioned techniques for particle handling require lab-on-a-chip devices[8–17] or complex transducer arrays.[16,27,28]

In recent years, new methods for particle manipulation have been realized by tailoring the acoustic field of artificial structures. Cai *et al.*[18] and He *et al.*[21] reported particle trapping and sieving by a one-dimensional (1D) periodic phononic crystal plate. Wang *et al.*[20] first experimentally realized acoustic patterning of particles in two-dimensional (2D) arrays assisted by a phononic crystal plate. With its structural flexibility, the acoustic artificial structure would provide a promising platform for particle manipulation. However, particle transport along a predefined pathway without moving the transducer or transducer array is still a challenge[24] with a lack of experimental realization. Here, we propose and implement a scheme for acoustically driven particle delivery assisted by an artificial structural plate with graded grating carved on one surface. Without moving the incident transducer, the acoustic amplitude field near the surface can be tuned to different positions by regulating the operating frequency, which originates from the grating with different heights corresponding to different resonant frequencies. Further, we demonstrate that the particles will transfer on the plate along a predefined pathway under the influence of the acoustic radiation force exerted by the gradient field.

To better illustrate the resonant transmission of a brass plate by varying the height of the gratings, we first study the transmission response of acoustic waves through a plate with periodical gratings (schematic structure shown in the inset of Fig. 1). A thin brass plate (thickness $t = 0.4$ mm) is patterned

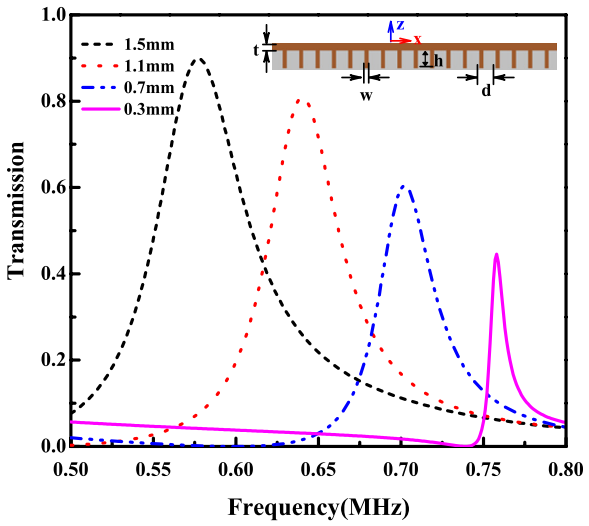

FIG. 1. Dimensionless transmission spectra of four uniform brass plates patterned with periodical gratings of different heights: 0.3 mm (pink solid line), 0.7 mm (blue dashed line), 1.1 mm (red dotted line), and 1.5 mm (black dashed line). A schematic view of a brass plate is shown in the inset.

a)Author to whom correspondence should be addressed: mzke@whu.edu.cn

with a periodical array of gratings (width $w = 0.3$ mm) with lattice constant d = 1.5 mm on the downside; the total length of the plate is $l = 58.5$ mm. In this work, COMSOL's Multiphysics (a finite-element analysis and solver software package) is adopted to numerically calculate the transmission spectra, field distributions, and acoustic radiation force (ARF), and a 2D geometric model is used in the simulation, where the material parameters are set as $\rho = 8600\,\text{kg/m}^3$, $c_l = 4400$ m/s, and $c_t = 2100$ m/s for brass and $\rho = 1000\,\text{kg/m}^3$ and $c_l = 1490$ m/s for water. Here, ρ, c_l, and c_t represent the density, longitudinal, and transversal sound velocities, respectively. The acoustic wave is initiated normally from downside of the sample (along the Z direction). Plane wave radiation conditions are set on both sides of the structure (along the X direction). As shown in Fig. 1, four transmission curves, respectively, correspond to a brass plate patterned with periodical gratings of different heights—0.3 mm (pink solid line), 0.7 mm (blue dashed line), 1.1 mm (red dotted line), and 1.5 mm (black dashed line)—all of which display a notable acoustic transmission peak with a distinct resonant frequency. As the height of the gratings increases, the transmission peak shows a red shift and a growth in amplitude. We can conclude that the transmission peak emerges from the resonance of the gratings and that different heights of the gratings will result in different frequency ranges. Therefore, based on this conclusion, we can modulate the acoustic field distribution with the position of the plate by designing the height of the gratings.

We designed a sample with the same parameters as illustrated in Fig. 1, while the height of the gratings varied with a gradient parameter. The three gratings of one height make up one group, the height of the group ranges from 0.3 mm to 1.5 mm with a height gradient of $\Delta h = 0.1$ mm, and the total structure comprises 13 groups. Figure 2(a) illustrates the side and top-down views of the plate with graded gratings on the downside, which are fabricated by a mechanical process.

Figure 2(b) shows the transmission spectra of the graded grating plate, where the blue solid line denotes the numerical simulation and the red dashed line indicates the experimental measurement. An ultrasonic transmission technique is adopted to conduct the experimental measurement.[29] The graded grating plate is fixed between a couple of high-intensity plane ultrasonic (HIPU) transducers, which have a central frequency $f = 0.5$ MHz, diameter D = 38.1 mm, and beam width W=25 mm. Because the transducer beam width W=25 mm is less than the plate length $l = 58.5$ mm, we measure the transmission in the middle of the plate. For consistency, we calculate the numerical transmission spectrum at the same position as the experimental measurement. Overall, the numerical and experimental transmission curves are consistent, as shown in Fig. 2(b), which demonstrates a wide transmission peak in the frequency range of 0.60–0.75 MHz. This wide transmission peak is caused by the graded grating structure, and it is worth noting that the middle height (0.5–1.3 mm) of the grating is primarily responsible, because the transmission spectra are focused on the middle portion of the sample. The amplitude of the wide transmission peak [Fig. 2(b)] is much lower than that of the periodical grating plate (Fig. 1), because of the energy distribution over a wide frequency range compared with the periodical structure with a sharp resonant transmission peak. The decreased smoothness of the simulated transmission at frequencies above 0.65 MHz [blue solid line in Fig. 2(b)] mostly comes from the structure between two unit groups, which, respectively, consists of three gratings. There is an abrupt change in the height, and usually the transmission in the high frequency range is easily affected by the parameters of the structure. Meanwhile, in the experiment, the structure does not have a guaranteed consistency as in the simulation; some imperfections in the structure reduced the abrupt changes of the height, which may have led to the smooth transmission [red dashed line in Fig. 2(b)] in the experiment. There is still a small discrepancy in the transmission amplitude between the numerical stimulation and the experimental measurement, which also stems from the imperfections in the structure, material absorption, and limited precision in the experimental measurement.

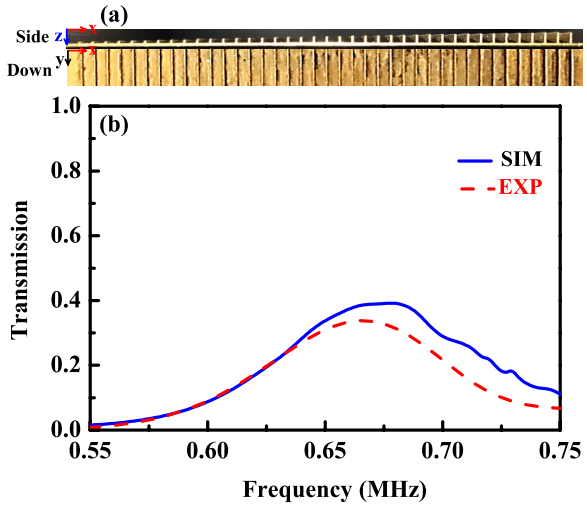

FIG. 2. (a) Side and top-down views of the sample fabricated by patterning graded rectangular gratings on the downside of the uniform brass plate. (b) Numerical simulated (blue solid line) and experimental (red dashed line) transmission on the plate.

Compared with the transmission spectra, the pressure field distribution will provide a more detailed acoustic response when an acoustic plane wave is initiated on this graded grating structure. In the numerical simulation, the Gaussian beam has a width of 25 mm from the bottom of the plate at the position of $x = 32.5$ mm. The pressure fields are measured as in Refs. 30–34. A HIPU transducer is used as a generating transducer, which is placed at the bottom of the water tank but at a distance of 30 mm from the plate. A receiving pinducer with a small diameter of 1.2 mm is used to scan the acoustic field in the X–Z plane and is controlled by a stepper motor. Figure 3 (Multimedia view) shows both the simulated (left) and measured (right) pressure field distribution for three frequencies, 0.63 MHz (a1) and (a2), 0.65 MHz (b1) and (b2), and 0.67 MHz (c1) and (c2), respectively. The results show that the transmission pressure field moves from the right position corresponding to the gratings with a large height toward the left position with a small height (along the negative X direction) as the frequency gradually increases from 0.63 MHz to 0.67 MHz. This clearly indicates that different resonant frequencies excite local acoustic fields at

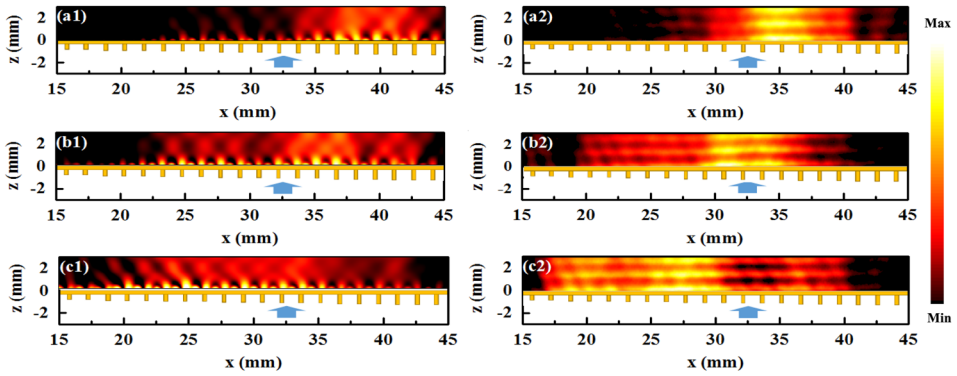

FIG. 3. Pressure field distributions of the graded grating plate for three different frequencies, where the left-hand images show the numerical simulation for the frequencies 0.63 MHz (a1), 0.65 MHz (b1), and 0.67 MHz (c1), and the right-hand images show the corresponding experimental measurement of the same frequencies, (a2), (b2), and (c2). The blue arrows point to the central position of the incident beam. (Multimedia view) [URL: http://dx.doi.org/10.1063/1.4991525.1]

different positions of the plate. See Multimedia view 1 for the detailed process.

Based on the properties of the field moving along the X direction on the grating plate, we further analyze the radiation force exerted on a steel particle ($\rho = 7670\,\mathrm{kg/m^3}$, $c_l = 6010\,\mathrm{m/s}$, and $c_t = 3230\,\mathrm{m/s}$) with a radius of 0.5 mm on the smooth surface of the graded grating plate. In the numerical calculation, the distance between the bottom of the cylindrical particle and the upper surface of the plate is $\Delta z = 0.1\,\mathrm{mm}$, according to the expression of the ARF acting on objects[18,20,21,35,36]

$$\mathrm{F} = -\oint_S \langle \mathbf{S} \rangle \cdot \mathrm{d}\mathbf{A},$$

where the differential area d**A** indicates the outer normal of a surface enclosing the particle and $\langle \mathbf{S} \rangle$ is the time-averaged Brillouin radiation stress tensor

$$\langle \mathbf{S} \rangle = \left[|p|^2/(4\rho_0 c_0^2) - \rho_0 |\mathbf{u}|^2/4 \right] \mathbf{I} + \rho_0 \mathrm{Re}(\mathbf{u}^* \mathbf{u})/2,$$

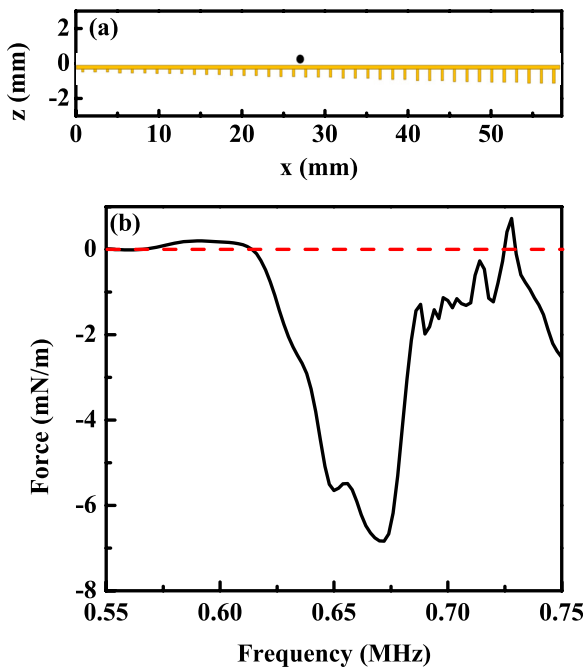

FIG. 4. (a) Schematic view of a uniform brass plate with graded gratings on the downside; a cylindrical steel particle (1 mm in diameter) is placed at $x = 27\,\mathrm{mm}$ on the topside of this structured plate. (b) Acoustic force along the X direction of the particle in (a). The red dashed line represents a zero acoustic radiation force.

where **I** stands for the unit tensor, ρ and c_0 represent the density and the sound speed of water, respectively, and **u** and p denote the first-order fluid velocity and pressure field on the surface of the particle, respectively. When the particle is placed on the top of the plate at position $x = 27\,\mathrm{mm}$ [as illustrated in Fig. 4(a)], the X-directional ARF $\mathrm{F_x}$ (black solid line) is exerted on a steel particle as shown in Fig. 4(b), where the red dashed line indicates the zero line. In the simulation, the Gaussian beam incident from the bottom of the plate has an amplitude of 1 MPa. Figure 4(b) demonstrates that the ARF is negative in the frequency range of 0.615–0.725 MHz, which corresponds to the wide transmission peak of Fig. 2(b). The negative ARF causes the particle to be attracted to the left position along the X direction. With the frequency gradually increasing from 0.62 MHz to 0.67 MHz, the negative ARF increases, which indicates that the particle can be driven to transfer along the plate from the effect of this acoustic force by tuning the working frequency. In other words, the particle will move to the left with a frequency increasing from 0.62 MHz to 0.67 MHz, and vice versa. An experimental demonstration is presented below.

Figure 6 (Multimedia view) shows the experimental demonstration of the acoustically driven particle transferring on the graded grating plate. The experimental setup is illustrated in Fig. 5. During the experiment, a signal is emitted from the HIPU transducer that is connected to a power amplifier (AG 1006) with an impedance matcher (50 Ω) with an electrical power input of 17 W. A specimen holder is used to fix the plate horizontally, and the distance between the plate and transducer is 30 mm. A digital camera is mounted to the top of the plate to record the process of the steel

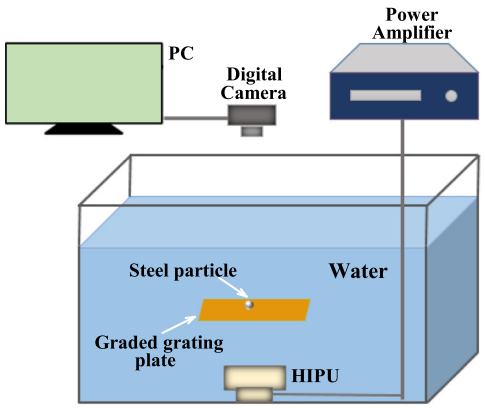

FIG. 5. Schematic diagram of the experimental setup.

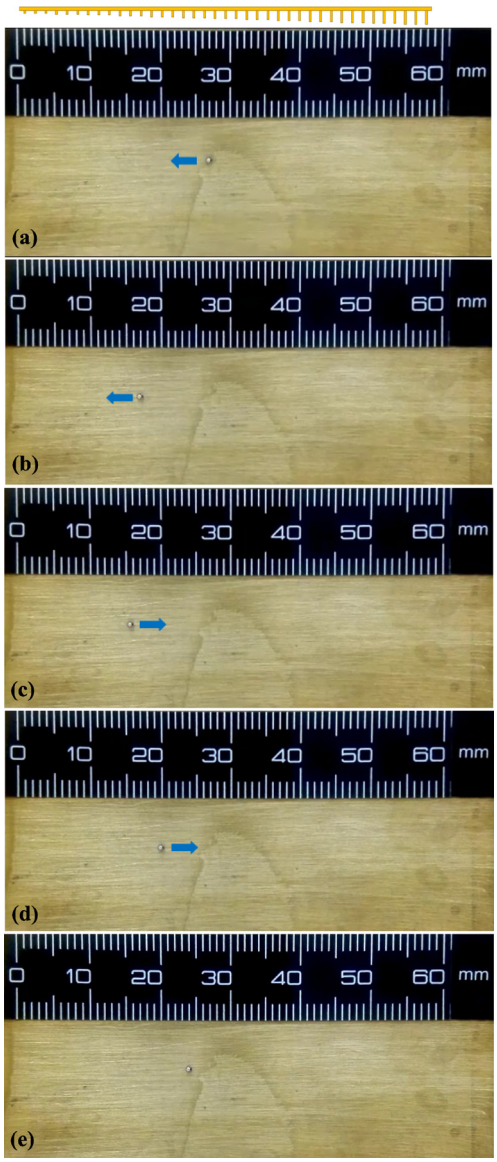

FIG. 6. Images of the acoustically driven process recorded by a digital camera. (a)–(c) Particle moving to the left with the frequency increasing from 0.63 MHz to 0.67 MHz; (c)–(e) particle moving back to the right with the frequency decreasing from 0.67 MHz to 0.63 MHz. The blue arrows represent the tendency of particle motion. The zero calibration in the five maps is at the leftmost part of the plate, as shown in the inset. (Multimedia view) [URL: http://dx.doi.org/10.1063/1.4991525.2]

particle transfer. To make a better experimental observation, we chose the working frequency range of 0.63–0.67 MHz. The particle is stationary at the starting point $x = 27$ mm without acoustic incidence with the amplitude power turned "OFF," as shown in Fig. 6(a) (Multimedia view). When the power is "ON," the particle begins to move as the frequency increases from 0.63 MHz to 0.67 MHz, and the particle moves to the left side (along the negative X direction), as shown in Figs. 6(b) and 6(c) (Multimedia view). When we decrease the frequency from 0.67 MHz to 0.63 MHz, the particle moves back along the positive X direction, as shown in Fig. 6(d) ($f = 0.65$ MHz) and (e) ($f = 0.63$ MHz) (Multimedia view). See Multimedia view 2 for the detailed process.

In conclusion, we have presented a comprehensive examination of acoustically driven particle delivery assisted by an artificial structural plate with graded grating carved on one surface. The grating with different heights corresponds to different resonant frequencies, and as a result, the graded grating plate has a wide transmission peak. This further leads to the pressure field moving along the X direction from the right position corresponding to the gratings with large height toward the left position with small height as the frequency gradually increases. This graded acoustic field will exert a negative ARF on a particle located on the plate, driving the particle to move along a predefined pathway simply by tuning the working frequency, instead of the traditional method of moving a transducer or transducer array. The proposed system has potential applications in acoustic manipulation and transportation.

This work was supported by the 973 Research Program of China (Grant No. 2015CB755500), the National Natural Science Foundation of China (Grant Nos. 11574233, 11504275, 11534013, and 11374233), and the National Science Fund for Talent Training in Basic Science (Grant No. J1210061).

[1]A. Ashkin, Phys. Rev. Lett. **24**, 156 (1970).
[2]J. Wu, J. Acoust. Soc. Am. **89**, 2140 (1991).
[3]J. Leach, G. Sinclair, P. Jordan, J. Courtial, and M. J. Padgett, Opt. Express **12**, 220 (2004).
[4]A. Jonáš and P. Zemánek, Electrophoresis **29**, 4813 (2008).
[5]K. Dholakia and T. Čižmár, Nat. Photonics **5**, 335 (2011).
[6]M. Dienerowitz, M. Mazilu, and K. Dholakia, J. Nanophotonics **2**, 021875 (2008).
[7]C. Min, Z. Shen, J. Shen, Y. Zhang, H. Fang, G. Yuan, L. Du, S. Zhu, T. Lei, and X. Yuan, Nat. Commun. **4**, 2891 (2013).
[8]X. Ding, S.-C. S. Lin, B. Kiraly, H. Yue, S. Li, I. K. Chiang, J. Shi, S. J. Benkovic, and T. J. Huang, Proc. Natl. Acad. Sci. U.S.A. **109**, 11105 (2012).
[9]X. Ding, Z. Peng, S.-C. S. Lin, M. Geri, S. Li, P. Li, Y. Chen, M. Dao, S. Suresh, and T. J. Huang, Proc. Natl. Acad. Sci. U.S.A. **111**, 12992 (2014).
[10]L. Meng, F. Cai, J. Chen, L. Niu, Y. Li, J. Wu, and H. Zheng, Appl. Phys. Lett. **100**, 173701 (2012).
[11]F. Guo, Y. Xie, S. Li, J. Lata, L. Ren, Z. Mao, B. Ren, M. Wu, A. Ozcelika, and T. Huang, Lab Chip **15**, 4517 (2015).
[12]D. J. Collin, B. Morahan, J. Garcia-Bustos, C. Doerig, M. Plebanski, and A. Neild, Nat. Commun. **6**, 8686 (2015).
[13]A. K. Tay, M. Dhar, I. Pushkarsky, and D. D. Carlo, Lab Chip **15**, 2533 (2015).
[14]C. E. Owens, C. W. Shields IV, D. F. Cruz, P. Charbonneau, and G. P. López, Soft Matter **12**, 717 (2016).
[15]V. Aubert, R. Wunenburger, T. Valier-Brasier, D. Rabaud, J.-P. Kleman, and C. Poulain, Lab Chip **16**, 2532 (2016).
[16]H. Mulvana, S. Cochran, and M. Hill, Adv. Drug Delivery Rev. **65**, 1600 (2013).
[17]L. Tian, N. Martin, P. G. Bassindale, A. J. Patil, M. Li, A. Barnes, B. W. Drinkwater, and S. Mann, Nat. Commun. **7**, 13068 (2016).
[18]F. Cai, Z. He, Z. Liu, L. Meng, X. Cheng, and H. Zheng, Appl. Phys. Lett. **99**, 253505 (2011).
[19]F. Li, F. Cai, Z. Liu, L. Meng, M. Qian, C. Wang, Q. Cheng, M. Qian, X. Liu, J. Wu, J. Li, and H. Zheng, Phys. Rev. Appl. **1**, 051001 (2014).
[20]T. Wang, M. Ke, S. Xu, J. Feng, C. Qiu, and Z. Liu, Appl. Phys. Lett. **106**, 163504 (2015).
[21]H. He, S. Ouyang, Z. He, K. Deng, and H. Zhao, J. Appl. Phys. **117**, 164504 (2015).
[22]C. Wang, F. Cai, F. Li, L. Meng, L. Geng, Y. Kang, and H. Zheng, in International Ultrasonics Symposium (2015).
[23]J. Lee, S. Y. The, A. Lee, H. H. Kim, C. Lee, and K. K. Shung, Appl. Phys. Lett. **95**, 073701 (2009).
[24]T. Wang, M. Ke, C. Qiu, and Z. Liu, J. Appl. Phys. **119**, 214502 (2016).
[25]Y. Li, C. Qiu, S. Xu, M. Ke, and Z. Liu, Sci. Rep. **5**, 13063 (2015).
[26]D. Baresch, J.-L. Thomas, and R. Marchiano, Phys. Rev. Lett. **116**, 024301 (2016).
[27]A. Marzo, S. A. Seah, B. W. Drinkwater, D. R. Sahoo, B. Long, and S. Subramanian, Nat. Commun. **6**, 8661 (2015).

[28]A. Marzo, A. Ghobrial, L. Cox, M. Caleap, A. Croxford, and B. W. Drinwater, Appl. Phys. Lett. **110**, 014102 (2017).
[29]M. Ke, Z. He, S. Peng, Z. Liu, J. Shi, W. Wen, and P. Sheng, Phys. Rev. Lett. **99**, 044301 (2007).
[30]J. Mei, B. Hou, M. Ke, S. Peng, H. Jia, Z. Liu, J. Shi, W. Wen, and P. Sheng, Appl. Phys. Lett. **92**, 124106 (2008).
[31]S. Peng, Z. He, H. Jia, A. Zhang, C. Qiu, M. Ke, and Z. Liu, Appl. Phys. Lett. **96**, 263502 (2010).
[32]S. Peng, X. Mei, P. Pang, M. Ke, and Z. Liu, Solid State Commun. **149**, 667 (2009).
[33]C. Li, M. Ke, S. Zhang, S. Peng, C. Qiu, and Z. Liu, J. Phys. D: Appl. Phys. **49**, 125304 (2016).
[34]X. Wu, X. Xia, J. Tian, Z. Liu, and W. Wen, Appl. Phys. Lett. **108**, 163502 (2016).
[35]C. Qiu, S. Xu, M. Ke, and Z. Liu, Phys. Rev. B **90**, 094109 (2014).
[36]S. Xu, C. Qiu, M. Ke, and Z. Liu, Europhys. Lett. **105**, 64004 (2014).